EFFECT OF THICKNESS OF SILICA SHELL COATED OVER AG NANOPARTICLES ON THERMAL, MECHANICAL, DIELECTRIC AND ELECTRICAL PROPERTIES OF PVA BASED COMPOSITES

Manoranjan Sethy[1*], Srikanta Moharana[2], Subash Ch. Sahu[3], Banarji Behera[4], R. N. Mahaling[5*]

Abstract

Silica coated Silver nanoparticles of different shell thickness dispersed in the polymer PVA were synthesized by a simple solution casting route for studying the effect of shell-thickness on the thermal, mechanical, dielectric and electrical properties of the resulting composites. In order to control the thickness of the Silica shell a slightly modified Stober method was adopted. The nanoparticles and the composites were characterized by XRD, FTIR, TEM, SEM, TGA**,** DSC and Impedance analyser to investigate the results. The TEM images revealed the average radius of the Ag nanoparticles at the cores to be 56 nm and the Silica shell thickness to be in the range of 31nm to 79nm. The FTIR study confirmed the coating of SiO_2 shell over the Silver core by identifying the characteristic chemical bonds. Results from various measurements confirmed that the thickness of the shell plays a key role in influencing different properties of the polymer composites. The dielectric constant of the composite was found to be maximum for the composite with minimum shell thickness and the data of dielectric constant versus thickness from experiments were compared with the data of a theoretical model. The as prepared composite with least thickness can be used as capacitors in energy storage devices.

Keywords: PVA (Polyvinyl Alcohol), Ag@SiO_2 core/shell, Polarisation, Dielectric Constant

[1]*Department of Physics, Bhadrak Autonomous College, Bhadrak, Odisha, India
Email: manoranjansethy2012@gmail.com
[2]School of Applied Sciences, Centurion University of Technology and Management, Odisha, India
[3]Department of Chemistry, Govt. Women's College, Sambalpur, Odisha, India-768001
[1, 4]Materials Research Laboratory, School of Physics, Sambalpur University, Jyoti Vihar, Burla-768019, Odisha, India
[1, 2, 5]Laboratory of Polymeric and Materials Chemistry, School of Chemistry, Sambalpur University, Jyoti Vihar, Burla-768019, Odisha, India

***Corresponding Author: -** Manoranjan Sethy
*Department of Physics, Bhadrak Autonomous College, Bhadrak, Odisha, India
Email: manoranjansethy2012@gmail.com

DOI: - 10.53555/ecb/2023.12.si10.00566

1.0Introduction

In recent times, Polymer Ceramic Composites with high dielectric constant and low dielectric loss have attracted wide attention of many researchers due to their potential applications in electronic and electrical industries in various forms such as capacitors, super capacitors, sensors, actuators, gate dielectric and electrical accessories etc[1–5]. These type of composites are fabricated by combining polymers such as PVDF (PolyVinylideneFlouride) and its Copolymer, PANI(Polyaniline) , PVA(Polyvinyl alcohol), PMMA(Polymethyl methacrylate) as host matrix and inorganic ceramics of high dielectric constant such as CCTO (Calcium Titanate) , BT(Barium Titanate), PZT(Lead Zirconium Titanate) etc. as reinforcements[6–10] .These composites have many advantages over the conventional inorganic high-k ceramic materials owing to easy processability, lightweight and low cost because of which these are in great demand for miniaturization of electronic devices in recent years[8].

So far, two effective synthesis routes have been widely used to prepare high k and low loss polymer ceramic composites[11]. One is the incorporation of high K inorganic ceramic particles into the host polymer[12] and the other is the incorporation of electrically conductive fillers i.e metal nanoparticles such as Au, Ag, Cu, Al, Zn, etc. and carbon fillers such as CB (carbon black), CNTS (Carbon Nanotubes), GNPS(Carbon Nanoplates) etc. into the electrically insulating polymers to prepare percolative composites[13–16]. Though, these two routes fulfil the main objectives, these two give rise to some drawbacks. In the first approach, the high loading of ceramics of volume fraction (usually >0.4) is required which in turn brings high dielectric loss and inevitably deteriorates the flexibility and mechanical performances of the composites[17]. Moreover, large dielectric constant contrast between ceramic nanoparticles and the polymer matrix will result in distorted electric field leading to a low breakdown field[18–20].

In the second approach, very high dielectric constant of the composite is achieved near the percolation threshold but the composites attain high value of dielectric loss and low dielectric breakdown field due to insulator-conductor transition near the percolation threshold which stands as a challenge to control.

In both these approaches while incorporating Nano fillers, uniform dispersion of fillers overcoming the agglomeration becomes a major concern. Since nano-fillers have very high surface area to volume ratio they have strong tendency to get agglomerated. So, in order to get the desired properties in the composites uniform dispersion of nano-fillers is the key target of many investigations.

Recently, incorporation of Core-shell nanoparticles in the polymer matrix is one of the significant advancements to control dispersion of nano fillers in the polymers[21–23]. Core Shell nanoparticles with metallic core and insulating shells have attracted wide attention owing to the stability of the core due to protection of the shell and isolation of the metallic nanoparticles from other metallic nanoparticles preventing aggregation. The thickness of the shell and the ratio between the radius of the core and thickness of the shell can be tuned to tailor different properties of the composite. The insulating shell coated over the metal core is found to be quite compatible with the polymer as it serves as an interface area between the metal and Polymer. The sudden fall in the dielectric constant of the metallic core from infinity to a very small value of dielectric constant of polymer is controlled by the insulating shell[12].

In the present study, for the synthesis of core-shell nanoparticles, Ag Nps have been chosen as core due to its excellent conductivity and surface Plasmon resonance behaviour and SiO_2 has been chosen as shell due to its low dielectric loss and good insulating property[8,21,24]. Moreover, Silica is a popular coating material used widely from a long time over the metallic core which not only enhances the colloidal stability but also prevents direct contact between the Ag nanoparticles at the core of one core-shell nanoparticles with those at the core of the other core-shell nanoparticles. In the present investigation, PVA (Poly vinyl Alcohol) has been chosen as the host polymer due to its biodegradability and high flexibility, tensile strength and excellent compatibility with Silica[25–27]. The silica shell here acts as a buffer layer between Ag nanoparticles and PVA in controlling the sudden drop in the values of the dielectric constant which in turn improves the dielectric breakdown field of the composite. Since the thickness of the shell plays a key role in controlling the property of the core shell nanoparticles, the effect of addition of Ag (core)–Silica (Shell) nanoparticles of different

thicknesses will definitely influence the thermal, mechanical, dielectric and electric properties of the composites formed after dispersion of such core-shell nanoparticles in the host polymer.

To the best of our knowledge, no investigation on the effect of variation of thickness of silica-shell coated over Ag core on the thermal, mechanical, dielectric and electrical properties of the PVA based composites have been reported in the literature. Here, we have prepared the composites through solution casting route controlling the thickness of Silica shell through stober method[28]. Objective of our study is to get polymer composite with increased dielectric constant and low dielectric loss along with improved dielectric breakdown.

2.0 Experiment

2.1Materials:

Silver nitrate($AgNO_3$), N,N-dimethyl formamide (DMF) ,50 % Dimethylamine (DA) aqueous solution, Tetraethyl orthosilicate (TEOS) and Poly(vinyl pyrrolidone) (PVP, Molecular weight: 40,000) were purchased from High Media ,India. Poly(vinylalcohol) of Molecular weight 89000-98000, 99+% hydrolysed, chemical formula [-CH_2CHOH-]$_n$ was purchased from Sigma Aldrich to be used as host polymer .

2.1.1 Synthesis of Ag nanoparticles

In a 250ml Flask, 100 ml of Ethylene Glycol (EG) was taken and the flask was refluxed for 1 hour and maintained at 150^0C. To this flask 0.25gm of $AgNO_3$was added and 1gram PVP was added slowly drop by drop. The mixture of the flask was stirred for one hour and then centrifuged at 10000 revolutions per minute. The entire mixture is now cooled and washed with acetone then dried at 100^0C for 12 hours to obtain Ag nanoparticles.

2.1.2 Synthesis of Ag @ SiO_2 Core-shell nanoparticles of different thickness

To control the thickness of silica shell over Silver core, Stober method was followed. Prepared Ag nanoparticles of certain amount were dissolved in certain amount of ethanol in a flask. To this mixture 50% Dimethyl amine (DA) was added in a particular proportion. The solution is then ultra-sonicated for half an hour. Three other such solutions were taken in three different flasks and all the solutions in the four flasks were added with four different amounts of TEOS and ammonia solution in the ratio of 1: 3: 6:10 and stirred for 12 h under room temperature. The solutions were then washed, centrifuged and dried at 60^0C for 8 hours to obtain four types of $Ag@SiO_2$ core-shell nanoparticles of different thickness which were named as $Ag@SiO_2(t_1)$, $Ag@SiO_2(t_2)$, $Ag@SiO_2(t_3)$, $Ag@SiO_2(t_4)$ nanopowders, where 't' is the thickness of the Silica shell.

2.1.3 Synthesis of PVA-20wt% $Ag@SiO_2$ composites of various thicknesses.

Four flasks were taken and certain amount of PVA was dissolved in 100ml of DMF in each flask. The solutions were stirred for 1 hour and then ultra-sonicated for half an hour. The synthesized $Ag@SiO_2(t_1)$, $Ag@SiO_2(t_2)$, $Ag@SiO_2(t_3)$, $Ag@SiO_2(t_4)$ nanopowders each of weight equal to 20wt% of PVA were taken in four different flasks and dissolved in DMF then stirred and sonicated for 2 hours until uniform dispersion was obtained. The dispersed solutions of $Ag@SiO_2(t_1)$, $Ag@SiO_2(t_2)$, $Ag@SiO_2(t_3)$, $Ag@SiO_2(t_4)$ nano -powderswere then added to the flasks containing the solution of PVA in four flasks. Now the solutions in these four flasks containing PVA-20wt%$AgSiO_2(t_1)$, PVA-20wt%$AgSiO_2(t_2)$,PVA-20wt%$AgSiO_2(t_3$) and PVA-20wt%$AgSiO2(t_4)$ were thoroughly stirred for 12 hours at 60 degree centigrade. The solutions were then transferred to four Petri Dishes and put in a hot air oven at 80^0C for 8 hours to get four films or composites.

3.0 Characterisation

The synthesized core/shell nanoparticles and composites were characterized by X-ray diffraction to identify the phase formation (Seifert 3000P X-ray diffractometer with CuKα radiation (λ = 1.5406 Å)) and diffraction reflections were recorded in the step of 0.02° with 1 Sec count time in every step 2θ scanning range of 10^0–90°. A Fourier transform infrared (FTIR) AVATAR360 (Thermo Nicolet, USA) was used in the wavenumber range 400-4000 cm^{-1} to detect the presence of functional groups. The morphology of the composites were investigated using a scanning electron microscope (SEM) Hitachi Regulus 8230. The size of nanoparticles and thickness of shell was further characterized using a TEM JEM-2100F (JEOL, Japan). DSC STA449C (Netzsch, Germany) was used to study the melting and crystallization behaviour. Thermal degradation behaviour was examined by thermo gravimetric analysis (TGA) using a TA Instruments Q500 from room temperature to 800°C at a heating rate 10°C/min. The tensile properties of the samples were determined using an Instron 5944 universal testing machine.Agilent 4294APrecision Impedance Analyser was used at

room temperature over the frequency 10 Hz to 10 MHz to carry out the dielectric measurements.

4.0 Results and Discussion

4.1 XRD

Figure 1 shows the XRD pattern of Ag nanoparticles. In this figure, five prominent peaks have been found at angles 2θ =38.18°, 44.35°, 64.5° and 77.43°, 81.68^0 which correspond to the miller indices (111), (200), (220) and (311) and (222)

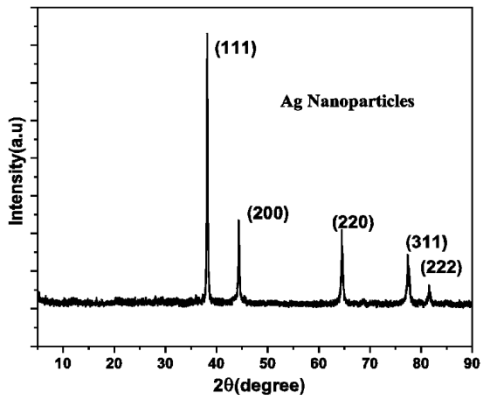

Figure 1 XRD spectrum of AgNps in the Braggs angle range 10^0 to 90^0

respectively. The peak at 38.18° is the most intense and the peak at 81.68° is the least intense. All the peaks match well with the standard reference pattern No (JCPDS #: 8-93-722) of FCC, Fm3m space group with cell parameter a=4.085 Å as analysed from the Xpert High Score software.

The particle size was obtained from the full-width at half maximum (FWHM) of the diffraction peaks using the Debye Scherrer formula[29] :

$$D = \frac{0.94\lambda}{\beta cos\theta} \qquad (1)$$

Where 0.94 is the shape factor due to spherical size of the nanoparticles,D = Crystallite size, λ=wavelength of Cu Kα radiation. β= Full Width at half maximum.2θ =Bragg's angle for peak position. Taking the four major peaks into consideration, the mean crystallite size was found to be 56 nm. The XRD parameters have been shown in the Table No.1

Table 1 (XRD parameters of Ag nanoparticles)

SL NO	Lattice parameters (A^0)	2theta (degree)	Miller indices (hkl)	d spacing(nm)	FWHM(β) In radians	Crystallite Size D (nm)	Mean Crystallite Size(D) (nm)
1	4.085	38.18	111	0.235	0.165	53.24	56nm
2	4.085	44.35	200	0.203	0.140	64.03	
3	4.085	64.5	220	0.144	0.160	61.35	
4	4.085	77.43	311	0.123	0.231	45.38	

Figures 2(a)-2(d) show the XRD spectrum of all the four composites loaded with different thickness of silica shell coated over the Ag core. A hump at $2\theta = 22.14^0$ corresponding to the miller index (101) which is the major characteristic peak of SiO_2 confirms the incorporation of Silica because of its amorphous nature[30]. However this peak gets broadened with increase in the thickness of the shell. Besides this peak no other peaks due to SiO_2 appear in the core shell nanoparticles .This may be attributed to the dominance of strong interaction of the AgNps in comparison to SiO_2.

It is found that the intensity due to different peaks decreases with increase in thickness of the shell; however there is neither any peak shifting nor any peak broadening corresponding to the silver nanoparticles.

The peak due to the miller index (222) shows diminishing intensity with increase in shell thickness in the composites.

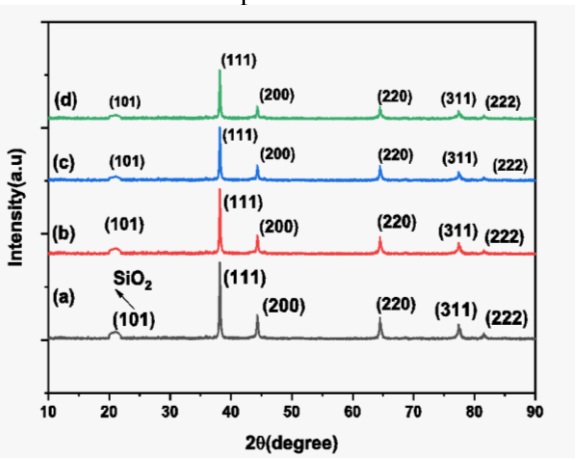

Figure 2 XRD spectrum of (a) PVA-20wt%Ag @SiO_2(31nm)(b)PVA –20wt%Ag@SiO_2 (53nm) (c) PVA–20wt%Ag@SiO_2 (72nm) (d) PVA – 20wt%Ag@SiO_2 (79nm)

4.2 FTIR

Figure 3 (a) shows the FTIR spectra of Ag@SiO_2 core-shell nanoparticles of thickness 31nm. The broad peak between 2900 cm^{-1} and 3450 cm^{-1} indicates the presence of hydroxyl group due to interaction of Ag nanoparticles with TEOS during preparation. The peak at 1627 cm^{-1} wave number represents Si-OH. The peaks at 1100 cm^{-1} and 598 cm^{-1} represent Si-O-Si stretching and bending respectively. The peak at 845 cm^{-1} and 550 cm^{-1} can be attributed to Si-O and Ag-O bonding. Hence all these peaks confirm the presence of SiO_2 in the core-shell nanoparticles and can be predicted that Ag nanoparticles have been well coated with SiO_2 layers.

Figure 3(b) shows the FTIR spectra of the composite with loading of Ag@SiO_2 core shell nanoparticles of thickness 31nm.The sharp peak at 3293 cm^{-1} represents the presence of OH group due to presence of the functional group in PVA. Besides this, the peaks at 2945 cm^{-1}, 2850 cm^{-1}, 1723 cm^{-1}, 1580 cm^{-1}, 1088 cm^{-1} can be attributed to CH_2 stretching, CH stretching, C=O, C=C & C-O bonds respectively which are the characteristic peaks of PVA confirming the presence of the Polymer PVA in the composite[31]. In the composite it is seen that the peaks due to the core-shell nanoparticles are not much dislocated which may be due to the strong interaction between Ag nanoparticles and SiO_2 layers.

However with increase in thickness of the shells it is seen that the peaks due to the Ag@SiO_2 nanoparticles start dominating while those due to the polymer PVA start diminishing.

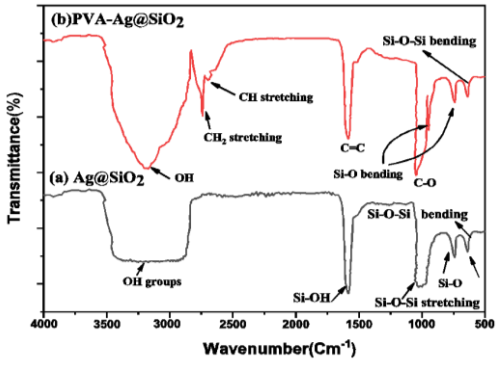

Figure 3. FTIR spectra of (a) Ag@SiO_2 core-shell nanoparticles of shell thickness 31nm (b) PVA-20wt% Ag@SiO_2 (31nm)

4.3 TEM

Figures 4(a)-4(d) show the TEM images of the four Ag@SiO_2 core-shell nanoparticles of different thickness on a 20nm scale. It is clearly seen that the Silica shell encapsulates the Ag cores which are almost spherical. Using ImageJ software it is confirmed that the average diameter of the Ag nanoparticles is 112nm and the average thickness of the silica layer in the samples is 31nm, 53nm, 72nm and 79nm respectively. The amount of TEOS has controlled the thickness of the Silica shell.

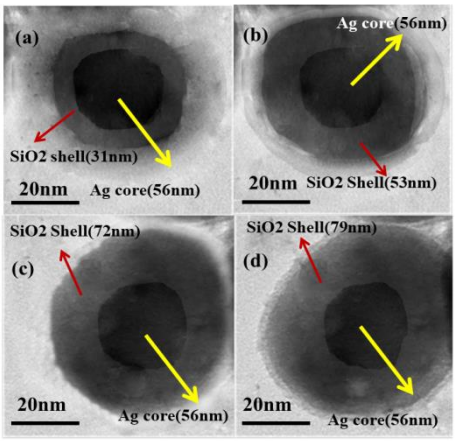

Figure 4 TEM Images of Ag@SiO_2 core-shell nanoparticles of (a) Ag core with average diameter 112 nm and shell thickness 31nm(b) Ag core with average diameter 112 nm and shell thickness 53nm(c) Ag core with average diameter 112 nm and shell thickness 72nm (d) Ag core with average diameter 112 nm and shell thickness 79 nm

4.4 SEM (Scanning Electron Microscopy)

Figures 5(a)-5(d) show the SEM microscopy images of the surfaces of the four composites with different Silica Shell thicknesses on a 4μm scale.

It is observed that with increase in the thicknesses of the Silica shell, agglomerations have increased and some cluster formations have been observed. There are a number of possible factors that contribute to the agglomerations in the composites. However, the reason can be ascribed to more importantly due to the stronger Van Der Waals forces that come into play between the Ag cores as with increase in thickness of the shell, distance between them decreases. It is seen that with increase in Shell thickness, the sizes of the particles have increased and there is gradual presence of more agglomerations which are quite obvious in the Figure 5(c) and then 5(d).The average size of the nanoparticles from the figure 5(a) to 5(d|) varies between 180nm to 290nm calculated from the Image J software.

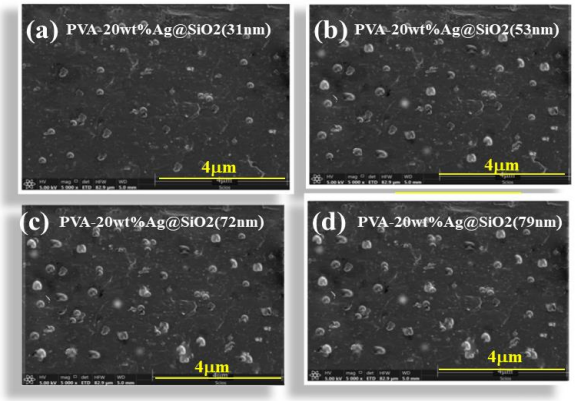

Figure 5. SEM images of (a)PVA-20wt%Ag@SiO_2 (31nm) composite (b) PVA-20wt%Ag@SiO_2 (53nm) composite (c) PVA-20wt%Ag@SiO_2 (72nm) composite (d) PVA-20wt%Ag@SiO_2 (79nm) composite

4.5 TGA Study (Thermal Properties)

TGA of PVA-20wt.%Ag@SiO_2 films are shown in Figure 6. It is seen that T_{onset}values of the composites increase with loading of thicker shells of Ag@SiO_2 core-shell particles. However these values are not higher than the $T_{onset}$of PVA rather much slightly lower. It can be seen that the composites exhibit higher stability than the neat polymer. The thermal stability of the PVA-20wt%Ag@SiO_2 composites with greater shell thickness are more stable .This is due to the fact that there is lesser air and voids in the composites. The results show that the prepared composites are promising candidates for high temperature resistant materials in the field of electronics, due to their high thermal stability.

Table-2 shows the initial decomposition temperature (T_{onset}), temperature for maximum rate of decomposition (T_{max}) and remaining amount of samples at 500°C (M_{500}). The data show that the composites with thicker shell are better thermally stable materials.

Table 2 (TGA Parameters of All samples)

Samples Name	T_{onset}(^{0}C)	T_{max}(^{0}C)	M_{500}(%)
Pure PVA	479	482	33
PVA -20wt% Ag@SiO_2(31nm)	472	485.96	44
PVA -20wt% Ag@SiO_2(53nm)	477	487.39	52
PVA -20wt% Ag@SiO_2(72nm)	478	493	59
PVA -20wt% Ag@SiO_2(79nm)	475	495	50

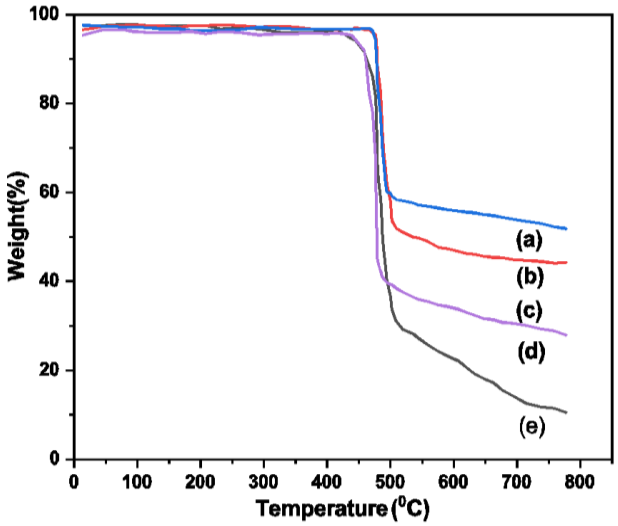

Figure 6 TGA of (a) PVA-20wt%Ag@SiO_2 (79nm) (b) PVA-20wt%Ag@SiO_2 (72nm)(c) PVA-20wt%Ag@SiO_2 (53nm) (d)) PVA-20wt%Ag@SiO_2 (31nm)

4.6 DSC (Differential Scanning Calorimetry)

The crystallization behaviour of PVA and PVA-20wt% Ag@SiO_2 composites with different thickness of silica shell was studied by differential scanning calorimetric at 10^{0}C/min from 30^{0}C to 200^{0}C. The DSC thermo grams (the first heating and second cooling traces were recorded) of PVA-20wt% Ag-SiO2 (t) composites are shown in Figure 7 and 8 the corresponding parameters are summarized in Table 3.

In the first heating endotherm of PVA, the peak around 186^{0}C corresponds to the melting point (T_m) of PVA. It is assumed that the Ag@SiO2

core-shell nanoparticles do not have impact on the melting behaviour of PVA after loading in the composites since the melting peaks do not vary in the composites. With increase in shell thickness of the core-shell nanoparticles, the enthalpy of the melting point decreases slowly. This decreasing trend is due to decrease in the crystallinity of the composites.

In the cooling cycle, the crystallization temperature (T_c) decreases with increase in the shell thickness of Ag-SiO_2 core-shell nano-particles. The decrease of T_c with increasing thickness indicates lower crystallinity of the composites than that of PVA as a result of the Ag@SiO_2 nanoparticles loading in the composites serving as anti-nucleating agents and hindering the crystallization of PVA in the composites.

The degree of crystallinity (Xc) can be calculated by using the following equation:

$$X_C(\%) = \frac{\Delta H_m}{\Delta H_0} \qquad (2)$$

Where $\Delta H_m$is the enthalpy of melting of the sample (J/g), ΔH_0=105 J/g is the enthalpy of fusion for 100% crystalline PVA. The calculated X_C results are also shown in Table 3.

Table 3 (DSC Parameters of PVA and PVA-20wt%Ag/SiO_2 (t) Composites**)**

Samples	ΔH_m(J/g)	T_m(^{0}C)	T_c(^{0}C)	X_c(^{0}C)
Pure PVA	**17.48**	**186.75**	**129.71**	**17.28**
PVA-20wt%AgSiO2(31nm)	**16.39**	**186.50**	**129.25**	**16.57**
PVA-20wt%AgSiO2(53nm)	**15.60**	**186.31**	**128.04**	**15.32**
PVA-20wt%AgSiO2(72nm)	**14.25**	**186.29**	**127.35**	**14.90**
PVA-20wt%AgSiO2(79nm)	**12.34**	**185.85**	**126.89**	**13.78**

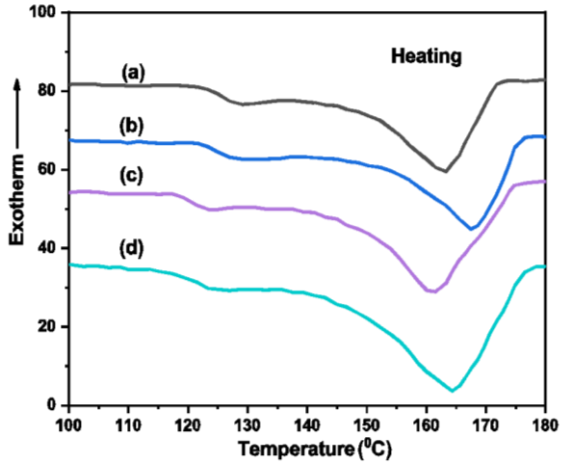

Figure 7 DSC thermograms of (a) PVA-20wt% Ag@SiO_2 (31nm) (b) PVA-20wt% Ag@SiO_2 (53nm)) (c) PVA-20wt% Ag@SiO_2 (72nm) (d) PVA-20wt% Ag@SiO_2 (79nm) during heating

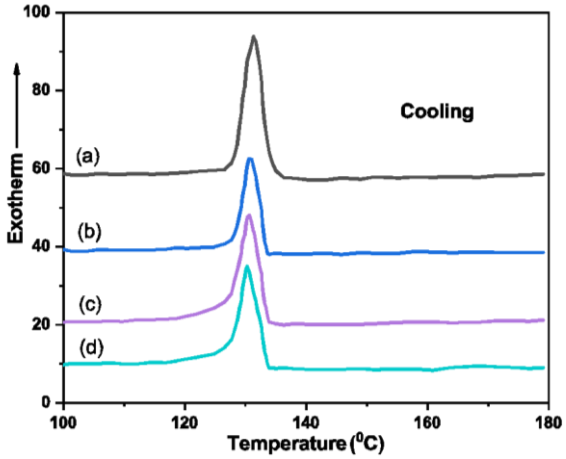

Figure 8 DSC thermo grams of (a) PVA-20wt% Ag@SiO_2 (31nm) (b) PVA-20wt% Ag@SiO_2 (53nm)) (c) PVA-20wt% Ag@SiO_2 (72nm) (d) PVA-20wt% Ag@SiO_2 (79nm) during cooling

4.7Tensile Parameters (Mechanical Properties)

The impact on the mechanical properties of the composites due to loading of Ag@SiO_2 core shell nanoparticles of different thickness was studied. The tensile properties measured were presented in Table 4. At a lower thickness of the shell, the tensile strength of the composites is close to the polymer PVA but at higher thickness due to more agglomerations the compact ness is reduced and consequently the tensile parameters are greatly affected. It is observed that the tensile strength decreases with increase in thickness due to weak compatibility between the polymer and the Ag core. This indicates that SiO_2 coating contributes to agglomeration of particles when it gets thicker over the Ag core. The Young's modulus for the PVA-20wt% Ag@SiO_2 (79nm) is 1285.4 MPa while it is 1209 MPa for Pure PVA film. The modulus of composites decreases due to its inhomogeneity and particle interactions.

Table 4 (Tensile parameters of PVA and the composites)

Sample	Tensile Strength (MPa)	Young's Modulus (MPa)	Elongation at Break (%)
Pure PVA	42.8 ± 2.9	1209.0 ± 84.6	11.4 ± 0.6
PVA-20wt%AgSiO_2(31nm)	47.5 ± 3.8	1761.2 ± 198.0	9.5 ± 1.0
PVA-20wt%AgSiO_2(53nm)	44.9 ± 3.9	1668.5 ± 175.4	6.9 ± 1.4
PVA-20wt%AgSiO_2(72nm)	44.5 ± 2.7	1378.4 ± 71.6	5.9 ± 1.7
PVA-20wt%AgSiO_2(79nm)	43.9 ± 1.5	1285.4 ± 77.2	5.4 ± 1.8

4.8 Dielectric Properties

Figure 9 shows the frequency dependence of dielectric constant of all four composites in the frequency range 10Hz to 10 MHz at room temperature. It is observed that the value of dielectric constant decreases with increase in frequency for all four composites with different thickness of shell. This is due to the fact that at low frequency all kinds of polarisation play roles and their resultant contributes to higher value of Dielectric constant but with rise in frequency contributions due to all kinds of polarisations start decreasing, hence the value of dielectric constant decreases[32]. In other words, with rise in frequency, the fast changing electric field fails to rotate the electric dipoles distributed randomly in the polymer making reduction in dipole moments per unit volume leading to which dielectric constant keeps on decreasing at higher frequency.

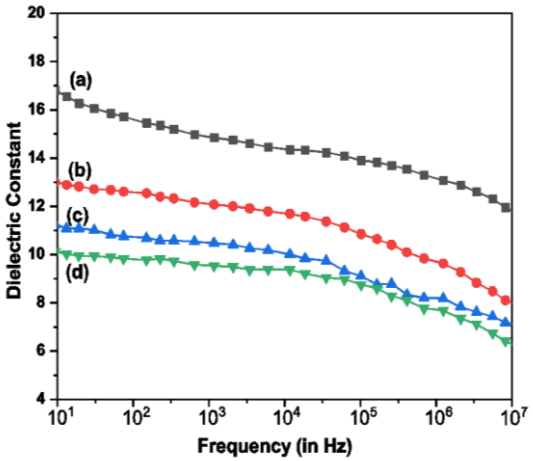

Figure 9 Dielectric constant versus frequency graph of (a) PVA-20wt% Ag@SiO_2 (31nm) (b) PVA-20wt% Ag@SiO_2 (53nm)) (c) PVA-20wt% Ag@SiO_2 (72nm) (d) PVA-20wt% Ag@SiO_2 (79nm) composites at room temperature.

Figure 10 shows how dielectric constant of all the four composites varies with thickness of SiO_2 shell at room temperature. It is found that dielectric constant of the composite increases with decrease in thickness of the shell. The explanation to this observation can be explained on the basis of a theoretical model as below[33] .

$$\varepsilon = \varepsilon_S \left(1 + \frac{d}{t}\right) \qquad (3)$$

Where ε_S =Shell thickness, d=diameter of the core, t=thickness of the shell

Table 5 Comparison of Theoretical values with Experimental values of dielectric constant versus thickness

Shell thickness in nm	Theoretical value of dielectric constant at 100HZ	Experimental value of dielectric constant at 100 Hz
31	18.54	17.12
53	12.45	13.7
72	10.22	11.45
79	9.67	10.23

From the equation (3) it is quite obvious that dielectric constant of the composite varies almost indirectly with the thickness of the shell. The data in the table 5 clearly shows the trend in the variation of the dielectric constant as a function of thickness of the silica shell.

The experimental values of the dielectric constant with decrease in the thickness of the shell shows similar trend though the values are not exactly the same as shown in the theoretical models. This is shown by the Figure 10

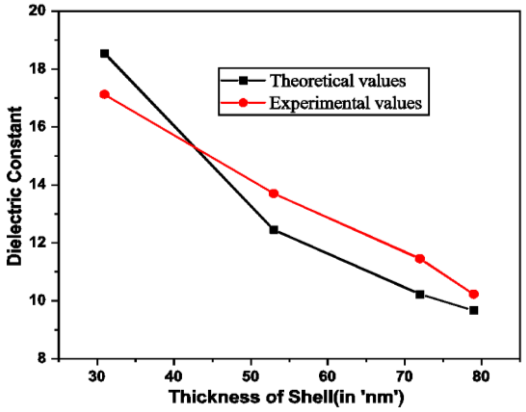

Figure 10 Dielectric Constant versus thickness of Silica Shell of the Composites at room temperature.

The increase in the value of dielectric constant of the composites due to decrease in thickness of the shell can be explained on the basis of mechanism as: the dielectric constant of the core-shell nanoparticles increases with decrease in shell thickness as per the equation[10]

$$\varepsilon_{eff} = \varepsilon_S \frac{\varepsilon_C(1+2\rho)+\varepsilon_S(1-\rho)}{\varepsilon_C(1-\rho)+\varepsilon_S(2+\rho)} \qquad (4)$$

Where, $\rho = \frac{R^3}{(R+R_i)^3}$ R is the radius of core and R_i is the thickness of the shell. Since Silver is a metal, its dielectric constant is ∞ and the Silica shell has dielectric constant roughly around 3.9[34] .It is observed that with rise in thickness of the shell ρ decreases and the effective dielectric constant approaches to the value of the shell. Hence it is found that the dielectric constant of the Ag@SiO_2 core-shell nanoparticles decreases with the increase in shell thickness. Considering effective medium theory, the effective dielectric constant of the system containing Ag@SiO_2 nanoparticles as one medium and the PVA polymer as another, the dielectric constant of the composite varies between the dielectric constant of both of these. On the basis of the interaction among each phase it can be explained that with reduction in shell thickness the interfacial area between the Ag core and the polymer PVA becomes more prominent resulting into higher polarisations and hence higher dielectric constant .On the basis of micro capacitor model it can be said that with decrease in shell thickness and the average diameter of the core remaining same, the thickness of the micro capacitor decreases giving more capacitance to the composite system and hence more dielectric constant for less thickness of shell.

4.9 Dielectric Loss

Figure 11 &12 show the dielectric loss of the composites as a function of frequency and thickness of the Silica shell respectively. It is observed that dielectric loss of the composites is least at 100 Hz frequency and maximum at 10MHz frequency. The trend is same for all the four composites. This decreasing trend can be explained as:

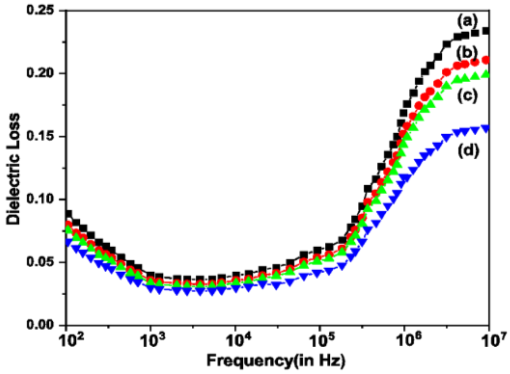

Figure 11 Dielectric Loss versus Frequency of (a) PVA-20wt%Ag@SiO_2 (79nm) (b) PVA-Ag@ SiO_2(72nm) (c)PVA-20wt%Ag@SiO_2(53nm) (d))PVA-20wt%Ag@SiO_2(31nm)

A number of factors may contribute to low loss at lower frequency. Since the silica shell is insulating in nature it does not interact with the electric field and hence the electrical conduction is reduced and there is minimum dissipation of energy contributing to low loss. Also, there is less movement of free electrons and the uniform dispersion of the core shell nanoparticles prevents the formation of conductive pathways leading to low loss.

At higher frequency, there is increased electronic conduction and the rapid changing electric field spends more energy to orient the trapped charges and hence the loss is high.

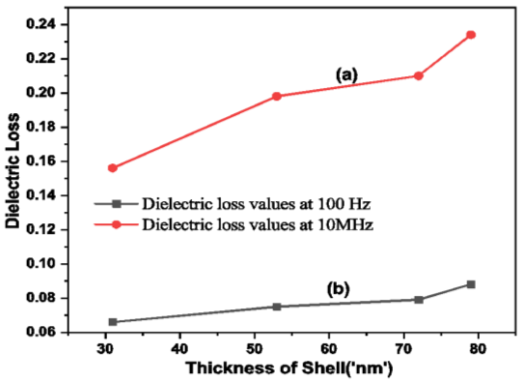

Figure 12 Dielectric Vs. Thickness of Silica Shell of all Composites at (a) 10MHz (b) 100 Hz

Figure 12 shows the variation of dielectric loss with thickness. From the graph it is concluded that Dielectric loss decreases with decrease in thickness of Silica shell. At a particular frequency and temperature, the dielectric loss of PVA-20wt%Ag@SiO_2 (31nm) is the lowest and that of PVA-20wt%Ag@SiO_2 (79nm) is highest. The reason to this cause can be explained as with decrease in thickness of silica shell interfacial area is decreased which reduces interfacial polarisation for which there exists fewer charge carriers .So the electric field does little work to orient the charges and hence the dielectric loss is very low. At 100 Hz and room temperature, the values of dielectric loss are 0.06 and 0.08 for PVA-20wt%Ag@SiO_2 (31nm) and for PVA-20wt%Ag@SiO_2 (79nm) respectively and these values are 0.15 and 0.23 at 10MHz respectively. Hence, by reducing thickness of shell low dielectric loss can be achieved.

4.10.Conductivity Study (Electrical properties)

Figure 13 shows the Conductivity versus Frequency of different Composites.

It shows that the conductivity of all the samples increases with increase in frequency. Possible reason may be that there are fewer free carriers in composites, which can be ignored compared with the conductivity produced by polarization at low frequency. With rise in frequency, the time period of the alternating electric field decreases at a faster rate which makes electric field to interact less with the disorderly free electrons to swift along its path enabling their freedom for mobility as a result of which there exists higher conductivity at higher frequency[35].

Figure14 shows the variation of electrical conductivity with decrease in thickness of the shell. It is found that conductivity of composites increases with decrease in shell thickens of the incorporated core shell Ag@SiO_2 nanoparticles keeping loading amount fixed at 20wt% of PVA. This trend can be explained due to the fact that with increasing thickness, the silica shell which is more insulating comes into more contact with the polymer as its interfacial area increases .The decreasing interfacial polarisation helps in the release of more free charges for the hopping of electrons from one spot to the other due to increase in distance between the core-shell nanoparticles. The electrical conductivity of **PVA-20wt%Ag@SiO_2(31nm)>PVA-20wt%Ag @SiO_2(53nm)>PVA-20wt%Ag@SiO_2(72nm) >PVA-20wt%Ag@SiO_2(79nm)** both at lower and higher frequency.

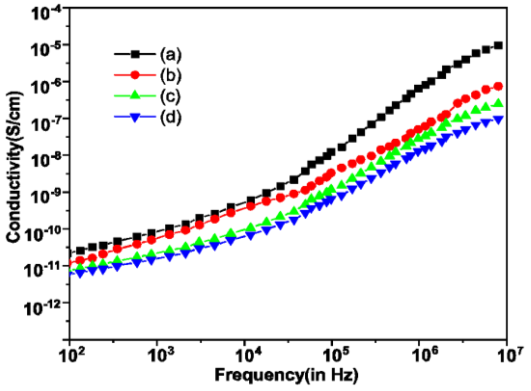

Figure 13 Variation of electrical conductivity versus frequency for (a) PVA-20wt% Ag@SiO_2 (31nm) (b) PVA-20wt% Ag@SiO_2 (53nm) (c) PVA-20wt% Ag@SiO_2 (72nm) (d) PVA-20wt% Ag@SiO_2 (79nm) composites at room temperature.

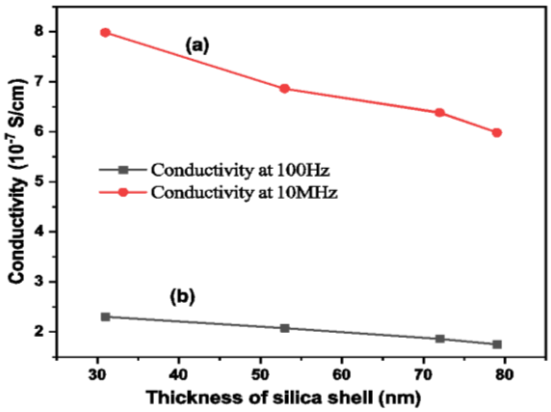

Figure 14 Variation of electrical conductivity versus thickness of Silica shell for (a) all composites at 10 Hz (b) all composites at 10MHz

5 .Conclusion

Ag@SiO_2 core-shell nanoparticles with different thickness of silica shell were prepared and controlled by different amount of TEOS. Taking 20wt% of PVA polymer as the weight of the Silica coated Ag Nps four composites with different thickness were synthesized for investigation. It was found that the thermal, mechanical, dielectric and electrical properties were affected by the thickness of the Silica shell .The value of dielectric constant of the Composite with thinnest silica shell attained 17.12 and closely matched with the computed value from the theoretical model considered. The variation of thickness of shell changes the interfacial area and interaction among the three phases of the composites which are the Polymer PVA, The Silica Shell and the Ag core. The Silica shell acts as a buffer layer to control sudden decline in dielectric constant and prevents the agglomeration of the Ag core particles. The synthesized composite with thinnest Silica shell showed reduced dielectric loss, improved electrical conductivity and enhanced dielectric constant which make it suitable for its application in energy storage devices.

.

References;

1. Huang, X., Sun, B., Zhu, Y., Li, S. & Jiang, P. High-k polymer nanocomposites with 1D filler for dielectric and energy storage applications. *Prog. Mater. Sci.***100**, 187–225 (2019).
2. Qiu, J. *et al.* Preparation and application of dielectric polymers with high permittivity and low energy loss: A mini review. *J. Appl. Polym. Sci.***139**, 52367 (2022).
3. Tan, D. Q. The search for enhanced dielectric strength of polymer-based dielectrics: A focused review on polymer nanocomposites. *J. Appl. Polym. Sci.***137**, 49379 (2020).
4. Wan, Y.-J. *et al.* Recent advances in polymer-based electronic packaging materials. *Compos. Commun.***19**, 154–167 (2020).
5. Zhou, L. & Jiang, Y. Recent progress in dielectric nanocomposites. *Mater. Sci. Technol.***36**, 1–16 (2020).
6. Shen, Y., Lin, Y., Li, M. & Nan, C.-W. High Dielectric Performance of Polymer Composite Films Induced by a Percolating Interparticle Barrier Layer. *Adv. Mater.***19**, 1418–1422 (2007).
7. Lei, T. *et al.* Excellent dielectric properties of polymer composites based on core-shell structured carbon/silica nanohybrid. *Appl. Phys. Lett.***103**, 012902 (2013).
8. Wang, R. *et al.* Core-shell structured $BATiO_3$ @ SiO_2 @ PDA for high dielectric property nanocomposites with ultrahigh energy density. *J. Appl. Polym. Sci.***138**, 50943 (2021).
9. Zhou, W. *et al.* Dielectric properties and thermal conductivity of core-shell structured Ni@NiO/poly(vinylidene fluoride) composites. *J. Alloys Compd.***693**, 1–8 (2017).
10. Quinsaat, J. E. Q., Nüesch, F. A., Hofmann, H. & Opris, D. M. Dielectric properties of silver nanoparticles coated with silica shells of different thicknesses. *RSC Adv.***3**, 6964 (2013).
11. Hao, X. A review on the dielectric materials for high energy-storage application. *J. Adv. Dielectr.***03**, 1330001 (2013).
12. Ji, W. *et al.* The effect of filler morphology on the dielectric performance of polyvinylidene fluoride (PVDF) based composites. *Compos. Part Appl. Sci. Manuf.***118**, 336–343 (2019).
13. Sebastian, M. T. & Jantunen, H. Polymer–Ceramic Composites of 0–3 Connectivity for Circuits in Electronics: A Review. *Int. J. Appl. Ceram. Technol.***7**, 415–434 (2010).
14. Shen, Y., Lin, Y., Li, M. & Nan, C.-W. High Dielectric Performance of Polymer Composite Films Induced by a Percolating Interparticle Barrier Layer. *Adv. Mater.***19**, 1418–1422 (2007).
15. Wang, C. *et al.* Synthesis, characterization and dielectric properties of Polyaniline@Ni0.5Zn0.5Fe2O4 composite nanofibers. *Mater. Sci. Semicond. Process.***40**, 140–144 (2015).
16. Arbatti, M., Shan, X. & Cheng, Z.-Y. Ceramic–Polymer Composites with High Dielectric Constant. *Adv. Mater.***19**, 1369–1372 (2007).
17. Balavijayalakshmi, J., Suriyanarayanan, N., Jayaprakash, R. & Gopalakrishnan, V. Effect

of Concentration on Dielectric Properties of Co-Cu Ferrite Nano Particles. *Phys. Procedia***49**, 49–57 (2013).
18. Boon, M. S., Serena Saw, W. P. &Mariatti, M. Magnetic, dielectric and thermal stability of Ni–Zn ferrite-epoxy composite thin films for electronic applications. *J. Magn. Magn. Mater.***324**, 755–760 (2012).
19. Bochenek, D., Niemiec, P., Skulski, R., Chrobak, A. &Wawrzała, P. Ferroelectric and magnetic properties of the PMN-PT-nickel zinc ferrite multiferroic ceramic composite materials. *Mater. Chem. Phys.***157**, 116–123 (2015).
20. Bochenek, D., Niemiec, P., Chrobak, A., Ziółkowski, G. &Błachowski, A. Magnetic and electric properties of the lead free ceramic composite based on the BFN and ferrite powders. *Mater. Charact.***87**, 36–44 (2014).
21. Fan, Y., Huang, X., Wang, G. & Jiang, P. Core–Shell Structured Biopolymer@$BaTiO_3$ Nanoparticles for Biopolymer Nanocomposites with Significantly Enhanced Dielectric Properties and Energy Storage Capability. *J. Phys. Chem. C***119**, 27330–27339 (2015).
22. Al- Ajeeli, A. F. H., Razeg, K. H. & Fuad Tariq, I. Copper At Silica Core - Shell Nanoparticles As Antibacterial Agents By Sol-Gel Chemical Methods. *3C Tecnol. Innov. Apl. Pyme***12**, 337–352 (2023).
23. Alimunnisa, J., Ravichandran, K. & Meena, K. S. Synthesis and characterization of Ag@SiO 2 core-shell nanoparticles for antibacterial and environmental applications. *J. Mol. Liq.***231**, 281–287 (2017).
24. Kar, E., Bose, N., Dutta, B., Mukherjee, N. & Mukherjee, S. MWCNT@SiO_2 Heterogeneous Nanofiller-Based Polymer Composites: A Single Key to the High-Performance Piezoelectric Nanogenerator and X-band Microwave Shield. *ACS Appl. Nano Mater.***1**, 4005–4018 (2018).
25. Jin, S. G. Production and Application of Biomaterials Based on Polyvinyl alcohol (PVA) as Wound Dressing. *Chem. – Asian J.***17**, e202200595 (2022).
26. Zhang, R., Xu, Y., Shen, L., Li, R. & Lin, H. Preparation of nickel@polyvinyl alcohol (PVA) conductive membranes to couple a novel electrocoagulation-membrane separation system for efficient oil-water separation. *J. Membr. Sci.***653**, 120541 (2022).
27. Udayakumar, G. P. *et al.* Biopolymers and composites: Properties, characterization and their applications in food, medical and pharmaceutical industries. *J. Environ. Chem. Eng.***9**, 105322 (2021).
28. Dos Santos Da Silva, A. & Dos Santos, J. H. Z. Stöber method and its nuances over the years. *Adv. Colloid Interface Sci.***314**, 102888 (2023).
29. Amutha, T., Rameshbabu, M., Muthupandi, S. & Prabha, K. Theoretical comparison of lattice parameter and particle size determination of pure tin oxide nanoparticles from powder X-ray diffraction. *Mater. Today Proc.***49**, 2624–2627 (2022).
30. Choi, G., Kim, J. & Kang, B. High Initial Coulombic Efficiency of SiO Enabled by Controlling SiO_2 Matrix Crystallization. *ACS Appl. Mater. Interfaces***14**, 44261–44270 (2022).
31. Sau, S. & Kundu, S. Variation in structure and properties of poly(vinyl alcohol) (PVA) film in the presence of silver nanoparticles grown under heat treatment. *J. Mol. Struct.***1250**, 131699 (2022).
32. Shoeb, M. *et al.* Investigating the size-dependent structural, optical, dielectric, and photocatalytic properties of benign-synthesized ZnO nanoparticles. *J. Phys. Chem. Solids***184**, 111707 (2024).
33. Shen, Y., Lin, Y., Li, M. & Nan, C.-W. High Dielectric Performance of Polymer Composite Films Induced by a Percolating Interparticle Barrier Layer. *Adv. Mater.***19**, 1418–1422 (2007).
34. Hu, Z. *et al.* Research progress of low dielectric constant polymer materials. *J. Polym. Eng.***42**, 677–687 (2022).
35. Sadiq, M. *et al.* Enhancement of Electro-chemical Stability Window and Electrical Properties of CNT-Based PVA–PEG Polymer Blend Composites. *ACS Omega***7**, 40116–40131 (2022).